Atmospheric Environment 208 (2019) 95–102

Contents lists available at ScienceDirect

Atmospheric Environment

journal homepage: www.elsevier.com/locate/atmosenv

Air quality impacts from the electrification of light-duty passenger vehicles in the United States

Jordan L. Schnell[a,b,c,*], Vaishali Naik[b], Larry W. Horowitz[b], Fabien Paulot[b,d], Paul Ginoux[b], Ming Zhao[b], Daniel E. Horton[a]

[a] Department of Earth and Planetary Sciences and Institute for Sustainability and Energy, Northwestern University, Evanston, IL, USA
[b] NOAA Geophysical Fluid Dynamics Laboratory, Princeton, NJ, USA
[c] Program in Atmospheric and Oceanic Sciences, Princeton University, Princeton, NJ, USA
[d] Cooperative Institute for Climate Science, Princeton University, NJ, USA

ARTICLE INFO

Keywords:
Electric vehicles
Air quality
Ozone
Particulate matter
Chemistry model

ABSTRACT

A central strategy in achieving greenhouse gas mitigation targets is the transition of vehicles from internal combustion engines to electric power. However, due to complex emission sources and nonlinear chemistry, it is unclear how such a shift might impact air quality. Here we apply a prototype version of the new-generation NOAA GFDL global Atmospheric Model, version 4 (GFDL AM4) to investigate the impact on U.S. air quality from an aggressive conversion of internal combustion vehicles to battery-powered electric vehicles (EVs). We examine a suite of scenarios designed to quantify the effect of both the magnitude of EV market penetration and the source of electricity generation used to power them. We find that summer surface ozone (O_3) decreases in most locations due to widespread reductions of traffic NO_x emissions. Summer fine particulate matter ($PM_{2.5}$) increases on average and largest in areas with increased coal-fired power generation demands. Winter O_3 increases due to reduced loss via traffic NO_x while $PM_{2.5}$ decreases since larger ammonium nitrate reductions offset increases in ammonium sulfate. The largest magnitude changes are simulated at the extremes of the probability distribution. Increasing the fraction of vehicles converted to EVs further decreases summer O_3, while increasing the fraction of electricity generated by "emission-free" sources largely eliminates the increases in summer $PM_{2.5}$ at high EV adoption fractions. Ultimately, the number of conventional vehicles replaced by EVs has a larger effect on O_3 than $PM_{2.5}$, while the source of the electricity for those EVs exhibit greater control on $PM_{2.5}$.

1. Introduction

The widespread electrification of the U.S. transportation sector offers the potential to simultaneously reduce greenhouse gas emissions, strengthen energy security, and improve air quality (Jacobson, 2009; IEA, 2018). However, the extent to which these benefits are realized – specifically for air quality – is largely dependent on the number and type of electric vehicles (EVs) that replace traditional internal combustion vehicles as well as the source of electricity generation used to power them (Requia et al., 2018). Here we investigate the air quality implications of a suite of EV transition and marginal electricity generation scenarios using a prototype version of the new-generation NOAA GFDL global Atmospheric Model, version 4 (GFDL AM4).

The exponentially increasing global market share of EVs (IEA, 2018) has prompted research on their efficacy in reducing greenhouse gases, but comparatively little effort has focused on their impact on air quality (Requia et al., 2018). This despite evidence that suggests air pollution impacts from the transportation sector exceed those from greenhouse gases (Delucchi, 2000; Hill et al., 2009; Michalek et al., 2011). A recent review article (Requia et al., 2018) concludes that a transition to EVs likely has greater potential to reduce emissions of gaseous pollutants (e.g., carbon monoxide (CO), nitrogen oxides (NO_x), volatile organic compounds (VOCs), sulfur dioxide (SO_2)) compared to particles (i.e., PM). Of the relatively few studies that have investigated the impact of EVs on ground-level ozone (O_3; seven identified by Requia et al. (2018)), most find that EVs will be a net benefit; however, the exact impact on O_3 is often dependent on location (e.g., urban vs. rural), season, and standing patterns in precursor emissions. The impact on air quality from the adoption of EVs can vary substantially between regions depending on existing transportation type and density (Huo et al., 2015), proximity to and type of power generation (Ji et al., 2012, 2015; Huo et al., 2013; Nichols et al., 2015), and the region's chemical regime

* Corresponding author. Department of Earth and Planetary Sciences, Northwestern University, Evanston, IL, USA.
E-mail address: jordan.schnell@northwestern.edu (J.L. Schnell).

https://doi.org/10.1016/j.atmosenv.2019.04.003
Received 29 November 2018; Received in revised form 22 March 2019; Accepted 2 April 2019
Available online 05 April 2019
1352-2310/

(e.g., NO_x-vs. VOC-limited for O_3 (Seinfeld, 1986), NH_3-rich vs. NH_3-poor for PM (Ansari and Pandis, 1998)). For example, states in the western U.S. (WUS) generally produce a larger fraction of their electricity from renewable and/or "emission-free" sources (i.e., solar, wind, hydroelectric, and nuclear) as compared to the eastern U.S. (EUS), where the electricity market is dominated by pollutant and precursor emitting combustion sources (i.e., coal, oil, natural gas, and biomass).

Most studies that have examined the impact of EVs report only changes in the total emissions associated with their adoption, but do not consider their spatial or temporal variation (Requia et al., 2018). For CO_2, a well-mixed greenhouse gas emitted by both conventional, internal combustion vehicles and electric generating units (EGUs), changes in its emissions can be directly related to changes in its atmospheric abundance, even if the location of the emissions are displaced by 100s of km (i.e., from the road to the power plant). The fate of the emissions of many air pollutants and their precursors, however, depends on additional factors including the proximity to, type, and magnitude of other nearby emissions sources, the relative rates at which co-pollutants are emitted, and even the season and time of day during which they are emitted. Thus to fully account for the complexity of changes to air pollution chemistry, emission changes should be used to drive a chemical transport model (CTM).

Several EV transition studies have employed a CTM over the U.S., mostly over smaller domains such as metropolitan areas (Alhajeri et al., 2011), regional air basins (Razeghi et al., 2016), or states (Brinkman et al., 2010; Thompson et al., 2011), but a few have used a CTM over the entirety of the continental U.S. as we do here (e.g., Tessum et al., 2014; EPRI, 2015; Nopmongcol et al., 2017). We expand on this work by first considering a wider range of more aggressive EV adoption scenarios (here, 25% and 75% compared to 10% (Tessum et al., 2014) or 17% (EPRI, 2015; Nopmongcol et al., 2017)), in line with some nations' legislated near-term electrification targets (IEA, 2018). Ambitious electrification targets provide the opportunity to examine potential chemical nonlinearities as well as assess the consequences of larger magnitude emission change signal. Similar to Tessum et al. (2014), we also explore the impact of the source of the marginal electricity demand (i.e., the additional electricity produced by EGUs on top of their baseload) by testing scenarios that range from a high-emission "combustion-only" scenario to an ambitious scenario that assumes a doubling of current marginal emission-free generation. Furthermore, we estimate the emission changes associated with an EV transition using a method that does not require the use of a power dispatch model, capacity expansion model, and/or economic model, all of which are typically close-guarded and proprietary (e.g., EPRI, 2015; Nopmongcol et al., 2017). Although there are multiple simplifications and assumptions, our emission remapping method is relatively simple and transparent, and thus can easily be implemented by other modeling groups using open-source data.

The paper is organized as follows: in Sect. 2 we describe the GFDL AM4 and the emission remapping method. Sect. 3 describes the results, where we evaluate the GFDL AM4, present our estimates of the emissions changes associated with a transition to EVs, and examine the model-simulated changes in surface air quality, from seasonal averages to the full probability distribution including extremes. Our conclusions and discussion are in Sect. 4.

2. Materials and methods

2.1. Model description

We use a developmental version of the new-generation NOAA Geophysical Fluid Dynamics Laboratory Atmospheric Model, version 4 (GFDL AM4) for our simulations (Zhao et al., 2018a, b). Details of the physical atmospheric model and changes from the previous version (AM3) are described in detail by Zhao et al. (2018a, b), although the prototype configuration of AM4 used here differs from that described in Zhao et al. (2018a, b). We double the horizontal resolution of the standard model setup; i.e., from ~100 km (96 × 96 grid boxes per cube face) to ~50 km (192 × 192), and we extend the model domain vertically, with 49 levels up to ~80 km (1 Pa) and a bottom layer thickness of about ~30 m. We also include a detailed online representation of tropospheric (and stratospheric) chemistry, updated from that in AM3 (Donner et al., 2011; Naik et al., 2013), and described by Schnell et al. (2018). To facilitate an evaluation of the model skill in simulating surface O_3 and $PM_{2.5}$, we nudge the model to NCEP-NCAR reanalysis winds using a pressure-dependent nudging technique and a relaxation time scale of 6 h at the surface and weakening to ~60 h by 100 hPa (Lin et al., 2012).

We model each of the major components of $PM_{2.5}$ individually and sum them to calculate the total mass of dry $PM_{2.5}$ (i.e., excluding aerosol water vapor) following Schnell et al. (2018). The major components include black carbon (BC), primary organic matter (OM), secondary organic aerosol (SOA), ammonium (NH_4^+), sulfate (SO_4^{2-}), nitrate, (NO_3^-), sea salt, and mineral dust. Anthropogenic SOA is assumed to be formed from C_4H_{10} by reaction with OH. Pseudo-emissions of biogenic SOA are parameterized as a 5% per carbon yield of offline emissions of isoprene and monoterpenes from vegetation. This simple formulation of biogenic SOA leads to a large overestimate of the OM component of $PM_{2.5}$ over the southeastern U.S. (see Fig. S1); however, lowering the yield further would result in unrealistically low values of global SOA production. All simulations use the same biogenic SOA source so although *BASE* is biased high, $PM_{2.5}$ absolute changes between experiments are unaffected (% changes are biased low).

For *BASE*, we integrate the model for two years (1 Jan 2013–31 Dec 2014) and discard the first year as spin up. Our sensitivity simulations branch off *BASE* on 1 Jan 2014 and are integrated for one year. Our base emissions dataset is that developed in support for the upcoming Coupled Model Intercomparision Project Phase 6 (CMIP6) (van Marle et al., 2017; Hoesly et al., 2017), which have a spatial resolution of 0.5° × 0.5° and a temporal resolution of 1 month.

2.2. Emission remapping algorithm

We construct an EV emissions dataset E^* by removing light duty passenger vehicle (LDPV) emissions and assigning new emissions according to extant power generation infrastructure and the fractional conversion to an EV fleet (Eq. (1)).

$$E^*_{s,t,j} = E^0_{s,t,j} - E^{LDPV}_{s,t,j} + E^{EGU}_{s,t,j} \quad (1)$$

where $E^0_{s,t,j}$ are the unmodified CMIP6 emissions of species s at time t and grid cell x_j, $E^{LDPV}_{s,t,j}$ are the emissions of LDPVs, and $E^{EGU}_{s,t,j}$ are the emissions of EGUs that power a fleet of EVs.

2.2.1. Emissions of gasoline and diesel powered LDPVs

We calculate the emissions of LDPVs as:

$$E^{LDPV}_{s,t,j} = fEV \cdot fE^{LDPV}_{s,j} \cdot E^{TRA}_{s,t,j} \quad (2)$$

where fEV is the simulation-dependent fraction of the LDPV fleet converted to EVs, $fE^{LDPV}_{s,j}$ is the fraction of transportation emissions associated with LDPVs and $E^{TRA}_{s,t,j}$ is the total transportation emissions in the CMIP6 dataset. For $fE^{LDPV}_{s,j}$, we use 2014 state-level speciated emission estimates from the National Emissions Inventory (US EPA, 2014), including BC, CO, NO, NH_3, OM, SO_2, and CH_2O. Estimates are also provided for a generic VOC category (Table S1), which we use as a proxy for species the model requires as input but without explicit LDPV fractions.

2.2.2. Emission from EGUs that power EVs

We calculate the EGU emissions that power EVs as:

$$E^{EGU}_{s,t,j} = ER^{EGU}_{s,j} \cdot V_{t,j} \quad (3)$$

where $ER_{s,j}^{EGU}$ is the average emission rate (g Wh^{-1}) of species s for the EGUs in grid cell x_j, and $V_{t,j}$ is the marginal electricity (Wh) generation assigned to grid cell x_j. We calculate $ER_{s,j}^{EGU}$ by identifying all EGUs of type biomass, coal, oil, and natural gas in the eGRID database (US EPA, 2017) and collocating them to a grid cell in the CMIP6 emission database. We only consider fossil fuel and biomass sources (hence, "combustion") to calculate the emission rate to allow for additional sensitivity simulations (see below). We determine the grid cell average emission rate for each modeled species as a weighted average of the individual EGU's emission rates with the weights equal to the EGUs' generating capacities. Each EGU has emission rates for NO and SO_2. Individual EGU emission rates for BC and OM are not available from eGRID so we calculate the emission rate at each grid cell using a weighted average of the mean emission rate (Cai and Wang, 2014) for the generation type (Table S2) and the weights equal to the EGUs' generating capacities. For model simulated species without published emission rates (mostly VOCs), we assume a conservative scaling factor equal to the lowest emission increase (associated with and only applied to energy production emissions) of the above four species. By only using combustion electricity generation sources to calculate our grid cell average emission rates, we can perform additional sensitivity simulations that vary the amount of emission-free electricity generation sources used to produce the additional electrical load needed to power the added EVs. Our primary simulation assumes all additional power is generated from extant combustion EGUs. For additional sensitivity simulations, we reduce the amount of added electricity at x_j (Eq. (4)) by the current fraction of electricity that is generated from emission-free sources (i.e., wind, water, solar, and nuclear) by state (US EPA, 2017; Table S1). On a state average level, this allows the current generation mix to produce any added electricity. We perform additional simulations by doubling the fraction of electricity produced by emission-free sources for all states (limiting to 100%). As this applies only to marginal generation, the 'doubling' can equivalently be thought of as either added renewable capacity (e.g., wind farm installation) or reduced combustion sources (e.g., retiring of coal plants).

2.2.3. New electricity generation requirement

The marginal electricity generated at a grid cell x_j required to power EVs at each of K grid cells x_k is:

$$V_{t,j} = \sum_{k=1}^{K} \left(w_{k,j}^{F} \cdot Q_{t,k} \cdot (1 - R_j)\right) \tag{4}$$

where $Q_{t,k}$ is the electricity required for transitioning a portion of the LDPV fleet to EVs, R_j is the fraction of emission-free generation sources for the state in which grid cell x_j is located in (equal to 0, the year 2014 fraction, or double the year 2014 fraction depending on the experiment; Table S1), and the cumulative weight $w_{k,j}^{F}$ is the combination of three individual weights (Eq. (5)). The individual weights are functions of distance (w^D, Eq. (6a)), whether the grid cells are within the same North American Electric Reliability Corporation (NERC) grid interconnection (w^R, Eq. (6b); https://www.eia.gov/maps/layer_info-m.php), and the available electricity generation capacity (w^W, Eq. (6c)). This weight formulation allows a grid cell x_j to produce electricity associated with the demand from grid cell x_k if (*i*) x_j and x_k are in the same NERC grid interconnection, and (*ii*) x_j has an existing combustion-based EGU. Note that for clarity in the notation of Eqs. (4)–(8), we refer to x_k as the grid cell where electricity is required and x_j as the grid cell where electricity is produced although the sets X = {x_1, x_2, …, x_k} and X = {x_1, x_2, …, x_j}are identical.

$$w_{k,j}^{F} = \left(w_{k,j}^{D} / \sum_{j=1}^{J} w_{k,j}^{D}\right) \cdot \left(w_{k,j}^{R} / \sum_{j=1}^{J} w_{k,j}^{R}\right) \cdot \left(w_{k,j}^{W} / \sum_{j=1}^{J} w_{k,j}^{W}\right) \tag{5}$$

$$w_{k,j}^{D} = \begin{cases} D^{-1} & \text{if } |x_j - x_k| \le D \\ |x_j - x_k|^{-1} & \text{if } |x_j - x_k| > D \end{cases} \tag{6a}$$

$$w_{k,j}^{R} = \begin{cases} 1 & \text{if } NERC_R(x_k) = NERC_R(x_j) \\ 0 & \text{if } NERC_R(x_k) \neq NERC_R(x_j) \end{cases} \tag{6b}$$

$$w_{k,j}^{W} = C(x_j) \tag{6c}$$

where D, a minimum distance parameter that prevents a singularity when x_j and x_k are the same grid cell (i.e., $w_{k,j}^{D} = \infty$, which would remap all of the additional electricity required from a grid cell to itself) is set to 50 km (roughly the size of a model grid cell). We also tested a value of D = 25 km, but it had only a minor effect on the remapped emission and resultant changes to the abundances of relevant species (not shown). The available generating capacity $C(x_j)$ is the difference between the total generating capacity and total electrical load of combustion EGUs in grid cell x_j.

2.2.4. Electricity requirement to power EVs

The electricity need for the EVs in grid cell x_k is calculated as:

$$Q_{t,k} = fEV \cdot VKT_{t,k}^{LDPV} \cdot (EV_{eff})^{-1} \cdot (1 - L)^{-1} \tag{7}$$

where $VKT_{t,k}^{LDPV}$ is the vehicle kilometers traveled by LDPVs in grid cell x_k, EV_{eff} is the efficiency ($kmW^{-1}h^1$) of a typical entry-level EV (Table S3), and L is the fraction of the marginal electricity lost in transmission (Table S3). We determine $VKT_{t,k}^{LDPV}$ using NO_x emissions from the transportation sector of the CMIP6 emission database as a proxy.

$$VKT_{t,k}^{LDPV} = fE_{NO_x,k}^{LDPV} \cdot E_{NO_x,t,k}^{TRA} \cdot \left(ER_{NO_x}^{LDPV}\right)^{-1} \tag{8}$$

where $fE_{NO_x,k}^{LDPV}$ is the fraction of transportation NO_x emissions associated with gasoline and diesel LDPVs (39), $E_{NO_x,t,k}^{TRA}$ is the NO_x emissions from the CMIP6 transportation sector, and $ER_{NO_x}^{LDPV}$ is the NO_x emission factor (g km^{-1}) of the replaced LDPVs. We choose a value for $ER_{NO_x}^{LDPV}$ = 0.96 gNO_x km^{-1}, which gives us a value of $\sum_{t=1}^{12}\sum_{k=1}^{K} VKT_{t,k}^{LDPV} = 3.3 \times 10^{12}$ km, in agreement with observations of total U.S. annual VKT (US DOT, 2017). Our $ER_{NO_x}^{LDPV}$ assumption is higher than an EPA reported value for gasoline fueled passenger cars and light trucks (0.693 gNO_x km^{-1}; (US EPA, 2008)), however, using this value also results in calculated NO_x reductions from transportation consistent with the NEI totals for LDPV. The emission rate discrepancy could be due to the EPA's exclusion of diesel powered vehicles, spatial variations in $ER_{NO_x}^{LDPV}$ not captured here, or simply an overestimation of NO_x transportation emissions in the CMIP6 database. Regardless, we utilize an $ER_{NO_X}^{LDPV}$ value that provides a $VKT_{t,k}^{LDPV}$ value and NO_x reductions consistent with observations.

2.2.5. Method caveats and assumptions

- Each EGU lists an additional emission factor for NO emitted during the "ozone season" (defined for each state; e.g., April to September). We performed one experiment that uses these "ozone season" values and found that several plant-level outliers of emission rates resulted in unrealistic "hotspots", so we only use the non-ozone season value for the remaining simulations.
- We assume EVs are charged and thus the marginal electric demand is co-located with where the EVs are driven. While this assumption may not be appropriate for finer resolution emission and/or modeling grids, it is likely not an important consideration for the ~50 km resolution of our model and emissions.
- Although rarely necessary, we assume that EGU generation capacity expands to accommodate the load when the marginal electrical load required to power the EVs exceeds extant available capacity.
- We do not consider the life-cycle emissions of EVs, such as the emissions associated with the production of the EVs' batteries; however, roughly half of those emissions occur outside of the U.S. (Tessum et al., 2014).
- The electricity generation mix is assumed to be constant throughout the year, and so, like the time-of-day charging effects (below), we do not account for daily, monthly, or seasonal variations in generation

mix (e.g., increased solar generation during summer and periods of clear skies).

- We also do not consider the time of day charging and its effects on EGU emission rates (e.g., Thompson et al., 2009; Weis et al., 2015). For example, EVs would likely predominantly be charged at night when fossil fuel sources make up a higher fraction of total electricity generation as compared to during the day (e.g., Zivin et al., 2014). In this case our grid-averaged emissions rates are likely biased low since the individual EGU emission rates are themselves a temporal average. Moreover, the impact on chemistry is drastically different for daytime vs. nighttime emissions of O_3 and $PM_{2.5}$ precursors. However, since anthropogenic emissions in the model are constant at each timestep within each month, we do not attempt to discern time of day generation and/or emissions.
- For LDPV emissions of BC and OM, we only remove those associated with vehicle exhaust, which we calculate as the difference between the total emissions and the non-exhaust component. We calculate the non-exhaust fraction using (*i*) the total $PM_{2.5}$ emission rates (Timmers and Achten, 2016) of brake wear, tire wear, and road dust suspension/resuspension (i.e., non-exhaust emissions – those that EVs emit), (*ii*) the fraction of BC and OM in each of the non-exhaust sources (Cai and Wang, 2014; Chen et al., 2012), and (*iii*) the assumption that 85% of total $PM_{2.5}$ emissions are from non-exhaust sources (Timmers and Achten, 2016). To be sure, since EVs are heavier than their conventional counterparts they would have higher non-exhaust emission rates (Simons, 2016), but we do not account for this here.

3. Results

3.1. Model evaluation

We evaluate the ability of the GFDL AM4 to simulate the abundances of species relevant to air quality using observations from surface monitoring networks in the U.S. and Canada. For ozone (O_3), we use hourly observations from the U.S. EPA's Air Quality System (AQS; https://www.epa.gov/aqs) and Clean Air Status and Trends Network (CASTNet; https://www.epa.gov/castnet) and Environment Canada's National Air Pollution Surveillance Program (NAPS; http://maps-cartes.ec.gc.ca/rnspa-naps/data.aspx). The hourly values are converted to the maximum daily 8-h average (MDA8) due to its use as a regulatory and health impact metric. For $PM_{2.5}$, we use daily average data from AQS and NAPS. Data for ammonium sulfate (NH_4SO_4), ammonium nitrate (NH_4NO_3), organic matter (OM, 1.6*OC), and black carbon (BC) are from the Interagency Monitoring of Protected Visual Environments network (IMPROVE; http://vista.cira.colostate.edu/Improve/). For O_3 and $PM_{2.5}$, we only use stations with data from at least 50% of the days in the season of interest. We only require data coverage of 16.7% of days for other species since they are typically only measured every third day.

Fig. S1 shows the summer (JJA) mean bias of *BASE* compared to station observations for MDA8 O_3 (Fig. S1a) and 24-h average $PM_{2.5}$ (Fig. S1b) and its major components (Figs. S1c–f). Fig. S2 show the analogous plots for winter (DJF). Regional averages are provided for the WUS (west of 100°W) and EUS (east of 100°W); this boundary is used for all regional average calculations. The model is biased high in summer MDA8 O_3 nearly everywhere, similar to many current global chemistry-climate models (e.g., Young et al., 2018). However, the correlation coefficient for daily MDA8 O_3 (Fig. S3) is greater than ~0.6 at most stations, indicating the model is correctly simulating the major processes that control surface O_3. Modeled $PM_{2.5}$ is mostly biased low except for the southeastern US and in parts of the Southwest. The high bias in the Southeast is due to excessive OM, specifically biogenic SOA, and thus does not affect the interpretation of our results since each experiment has the same biogenic SOA. The high bias in the Southwest is accompanied by consistently negative correlation coefficients (Fig. S3), possibly indicating a misrepresentation of dust emissions since dust is a dominant component (~50%) of $PM_{2.5}$ in the region and the emissions are a function of wind speed and thus can have substantial daily variability (Ginoux et al., 2001). $(NH_4)_2SO_4$ is biased low in most locations, particularly over the EUS (NMB = −22%) where significant coal-fired electricity generation occurs. The summertime bias for NH_4NO_3 is generally near-zero or negative, however, summer abundances (both modeled and observed) are typically low due to its thermal instability. The bias in winter (Fig. S12*D*) is positive and much larger in magnitude (NMB = 106%) compared to summer, possibly resulting from inadequate surface NO_3^- removal (Paulot et al., 2016). As such, any simulated reductions in NH_4NO_3 may be exaggerated. Beyond the six species we have evaluated here, similar configurations of the GFDL model have been recently evaluated in their ability to simulate pollution and relevant chemistry, demonstrating its wide use and utility: e.g., sulfate and conversion of SO_2 to sulfate (Paulot et al., 2016); nitrate and ammonia (Paulot et al., 2017) and NO_x, NO_y, HNO_3, and several VOCs (Li et al., 2018).

3.2. Experiments and associated annual emission changes

We performed six model simulations with GFDL AM4 for the year 2014 designed to span a range of hypothetical EV market penetrations and marginal electricity generation types (Table 1). We refer to the experiments as *eX-rY*, where *X* is the percentage of gasoline- and diesel-powered light-duty passenger vehicles (LDPVs) converted to EVs (either 25% or 75%), and *Y* denotes the emission-free (i.e., solar, hydro, wind, and nuclear) generation of marginal electricity (i.e., only that required to power the EV fleet), which can be *0* (marginal electricity demand generated solely by combustion sources), *C* (EVs are powered by the *current* electricity generation mix for each state), or *2C* (each state's emission-free fraction is doubled). We focus the presentation of our results on the scenario with 25% adoption of EVs with a doubled current fraction of emission-free generation, hence *e25-r2C,* which is likely closest to similar studies' design and market-projected near-term future (e.g., Tessum et al., 2014; EPRI, 2015; Nopmongcol et al., 2017; IEA, 2018). We note, however, that direct comparisons to other studies should be made with caution due to wide-ranging assumptions and experimental setup. We refer to the control simulation as *BASE*.

The annual total anthropogenic emission changes (Mg yr^{-1}) of NO, SO_2, organic matter (OM), black carbon (BC), CO, and C_4H_{10} (n-butane, see below) for the *e25-r2C* experiment compared to *BASE* are shown at each 0.5° × 0.5° grid cell of the native emissions in Fig. 1a–e, respectively. Relative (%) changes are shown in Fig. S4, absolute changes for all experiments for these six species are shown in Fig. S5, and regional average relative and absolute changes are provided in Tables S4 and S5, respectively, for each experiment and each species emitted in the model.

Emission decreases are widespread for all species, with the largest decreases throughout the eastern urban corridor, major metropolitan areas, and highly-trafficked areas of the west coast (Fig. 1). Although

Table 1
Summary of modeling experiments.

Name	% EV	Renewable Fraction[a]
BASE	0	n/a
e75-r0	75	0
e75-rC	75	2014
e75-r2C	75	2*2014
e25-r0	25	0
e25-rC	25	2014
e25-r2C	25	2*2014

[a]0 = combustion only (i.e., only coal, oil, gas, and biomass).
[a]2014 = year 2014 state-level emission-free generation.
[a]2*2014 = double year 2014 values (≤100%).

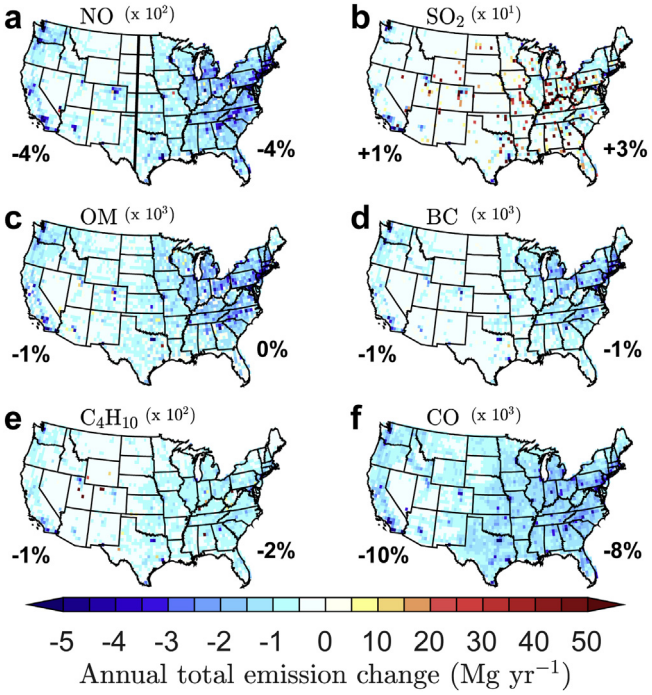

Fig. 1. Spatial patterns of the *e25-r2C* scenario annual total anthropogenic emission changes (Mg yr^{-1}) for (a) NO, (b) SO_2, (c) OM, (d) BC, (e) C_4H_{10}, and (f) CO. Regional average percent changes are provided for the WUS (west of 100°W) and EUS (east of 100°W). Note that each species has a scaling factor at the top of the plot (e.g., 10^2 for NO) and that positive side of the colorbar is 10 times the negative side; the black line in (a) is 100°W.

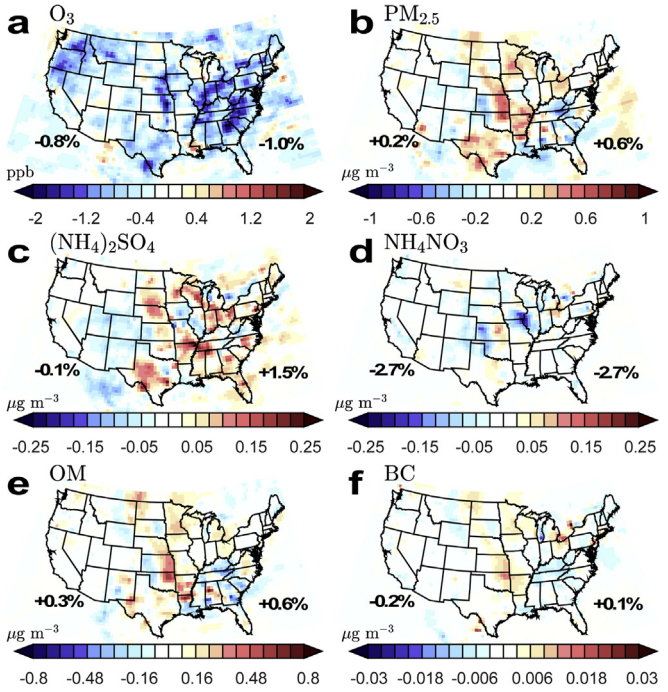

Fig. 2. Spatial patterns of the *e25-r2C* scenario summer (June-July-August) changes in (a) MDA8 O_3, and daily average (b) $PM_{2.5}$, (c) $(NH_4)_2SO_4$, (d) NH_4NO_3, (e) OM, and (f) BC. Units for MDA8 O_3 are ppb, all others are μg m^3. Regional averaged percent changes are provided for the WUS (west of 100°W) and EUS (east of 100°W).

most grid cells show decreases (> 80% of grid cells for each species), the positive changes (where electricity generation occurs) are up to 10 times the magnitude (note the color bar scale) and largely offset the reductions in traffic emissions on a regional average, at least for species emitted by the power generation sector. For NO_x, we estimate anthropogenic emission decreases of about 4% (~0.3 Tg) for the *e25-r2C* scenario. For SO_2, which is emitted in relatively small quantities from the transportation sector (mostly from diesel fuel combustion), emissions increase by ~2% (~0.1 Tg) over the U.S. as a whole, consistent with some previous work on EV adoption over the U.S. (Nichols et al., 2015) and elsewhere (Li et al., 2016; Wu and Zhang, 2017). While some western states have relatively large increases in SO_2 emissions (e.g., Colorado), the bulk of the increase occurs along the Ohio River Valley and the eastern urban corridor where vehicle density is high (i.e., increasing the amount of electricity need) and where coal supplies a large fraction of electricity generation. While our estimate that SO_2 emissions increase following partial electrification agrees with most prior work (Requia et al., 2018), one study finds a decrease (Nopmongcol et al., 2017); however they model the year 2030 when EGU SO_2 emissions are assumed much smaller while our experiments assume no modifications to the power generation sector. Emissions changes for C_4H_{10}, which in the model represents hydrocarbons with four or more carbons excluding isoprene and terpenes, are shown since its abundance directly impacts the formation of modeled anthropogenic secondary organic aerosol (SOA). C_4H_{10} emissions decrease at most grid cells and on average over both the EUS (−2%) and WUS (−1%). Nopmongcol et al. (2017) model large VOC reductions in emissions from hydrocarbon fuel refinery, which we and others (e.g., Tessum et al., 2014) do not; and thus we may underestimate the total VOC reduction. This emission source, like the production of EV batteries (Tessum et al., 2014), is likely an important source of uncertainty and will be investigated in subsequent research. CO emissions have the largest relative (−9%) and absolute (−3 Tg yr^{-1}) decrease since the transportation sector is its largest source and it is emitted only in small quantities by the power generation sector. Emission changes for other scenarios are similar in pattern but vary in magnitude (Fig. S5).

3.3. Seasonal average changes

Fig. 2 shows the changes in summer (June–July–August) average maximum daily 8-h average (MDA8) O_3, and daily average fine particulate matter ($PM_{2.5}$) and its major constituents for the *e25-r2C* experiment. Changes for winter (discussed below) are plotted in Fig. S6; changes for each season and experiment are shown spatially in Figs. S7–S12 and averaged over regions in Table S6.

Widespread summer O_3 decreases are simulated (up to ~1–3 parts per billion (ppb), Fig. 2a), largely following the pattern of relative reductions in NO_x (Fig. S4a). Indeed, the largest decreases occur in the Pacific Northwest and the Mid-Atlantic states where both the LDPV fraction of transportation NO_x (Table S1) and overall NO_x reductions (Fig. 1a) are largest. Both odd oxygen (O_x = O + O_3) production ($P(O_x)$) and loss ($L(O_x)$) decrease at the surface during summer in all scenarios and in both regions (Fig. S13), but O_3 abundances decrease since reductions in $P(O_x)$ are about 50% larger than the reductions in $L(O_x)$. Only a few grid cells do not see O_3 decreases; i.e., in locations where newly allocated marginal power generation significantly increases NO_x emissions (e.g., northern Missouri and southwestern Wyoming; Fig. 1a and Fig. S4a), or where O_3 production is likely VOC-limited (e.g., southern California (Duncan et al., 2010)) or both (Las Vegas area). On a regional average, both the WUS and EUS become more NO_x-limited during summer, with the surface CH_2O/NO_2 ratio (Jin et al., 2017) increasing by ~3% (~10%) for the *e25-r0/C/2C* (*e75-r0/C/2C*) scenarios (Fig. S13). Summer average O_3 also decreases nearly everywhere even when all of the marginal electricity is generated by combustion sources (*e25-r0*); in fact, summer O_3 decreases on average in all of our scenarios (Table S6).

The changes in total $PM_{2.5}$ (Fig. 2b) are the sum of the changes in its components (Fig. 2c–f), which often conflict in sign due to their

differing emission sources and chemical controls. Overall, total summer $PM_{2.5}$ for *e25-r2C* increases slightly on average over both the WUS and EUS due to increased $(NH_4)_2SO_4$ and OM. Indeed, the abundance of summer surface SO_2 (a hazardous air pollutant and precursor to $(NH_4)_2SO_4$) increases by ~3% over the EUS for *e25-r2C* and over 15% for *e75-r0* (Fig. S13b). The effect of electricity generation mix on resultant $PM_{2.5}$ is especially evident over Illinois, which is largely insulated from the increased $PM_{2.5}$ of adjacent states due to its large current (51%) and doubled (100%) renewable generation fraction. Increasing the amount of combustion generation generally results in greater increases in $PM_{2.5}$ (Fig. S8). One exception is summer averaged over the WUS, where the *e75-r2C* scenario has a larger positive $PM_{2.5}$ change compared to the *e75-rC* scenario (Table S6) despite fewer emissions of all species in the *e75-r2C* scenario (Table S5). We hypothesize that this is due to nonlinear chemistry from wildfire OM emissions stretching from northeast Montana through Arkansas.

Changes in OM are positive in the central U.S. and a northern swath from eastern Montana to New York, while the changes are negative over most of the southeast. BC changes are closely related spatially to OM changes but are about an order of magnitude smaller. Although biogenic SOA (counted as part of OM) is constant among the experiments here, it would likely increase in many locations due to increases in SO_2 emissions (Fig. 1b) and the associated enhancement of acid-catalyzed aqueous-phase SOA formation from isoprene epoxydiols (IEPOX) (Marais et al., 2016).

Overall, winter O_3 changes for *e25-r2C* (Fig. S6a) are mostly small and positive (~1 ppb), but small decreases occur in remote regions. The largest winter increases occur in regions with the largest summer reductions – namely the Mid-Atlantic states and the eastern urban corridor. For more aggressive adoption scenarios (i.e., those with greater NO_x reductions), increases are found in areas with ample winter insolation – e.g., Florida, Texas. The winter O_3 increase is due to reduced $L(O_x)$ (Fig. S14), likely via reduced titration by traffic NO since the *e75-r0/C/2C* scenarios have increased $L(O_x)$ compared to the *e25-r0/C/2C* scenarios.

Winter $PM_{2.5}$ decreases occur nearly everywhere (Fig. S6b) and result from much larger reductions in NH_4NO_3 in winter compared to summer due to the enhanced thermal stability of NH_4NO_3 in colder temperatures (Stelson and Seinfeld, 1982). Similar to summer, $(NH_4)_2SO_4$ abundances increase in winter and are again largest over the EUS due to heavy reliance on coal-fired power generation. Both winter OM and BC decrease on average, but there are highly localized areas with large increases – specifically OM, which is likely a combination of biomass-powered electricity generation and relatively shallow, stable boundary layers that confine pollution near the surface.

3.4. Extreme changes

Besides average seasonal changes, it is also important to examine changes over the full probability distribution – particularly at the extremes – since the highest pollutant abundances have disproportionate impacts on ecosystem and human health (IPCC, 2014) and often coincide with other extremes such as heat waves (Schnell and Prather, 2017). Fig. 3 shows each scenario's changes relative to *BASE* binned at every 10th percentile for O_3, $PM_{2.5}$, NH_4NO_3, and $(NH_4)_2SO_4$, averaged over the WUS and EUS separately. Relative changes are shown in Fig. S13.

Changes in O_3 (Fig. 3a–b) are almost entirely negative for both averaging domains and all scenarios except for the lowest percentiles (i.e., cleanest winter days). The magnitude of the decrease is largely determined by the number of conventional vehicles replaced by EVs and thus NO_x emission reductions, with the *e75* scenarios (red/yellow lines) showing much larger O_3 decreases than the *e25* scenarios (blue lines). The source of electricity generation only has a notable impact on O_3 for the *e75* scenarios at high percentiles over the EUS, with the *e75-r2C* scenario having the largest O_3 benefit (~2 ppb). An EV transition

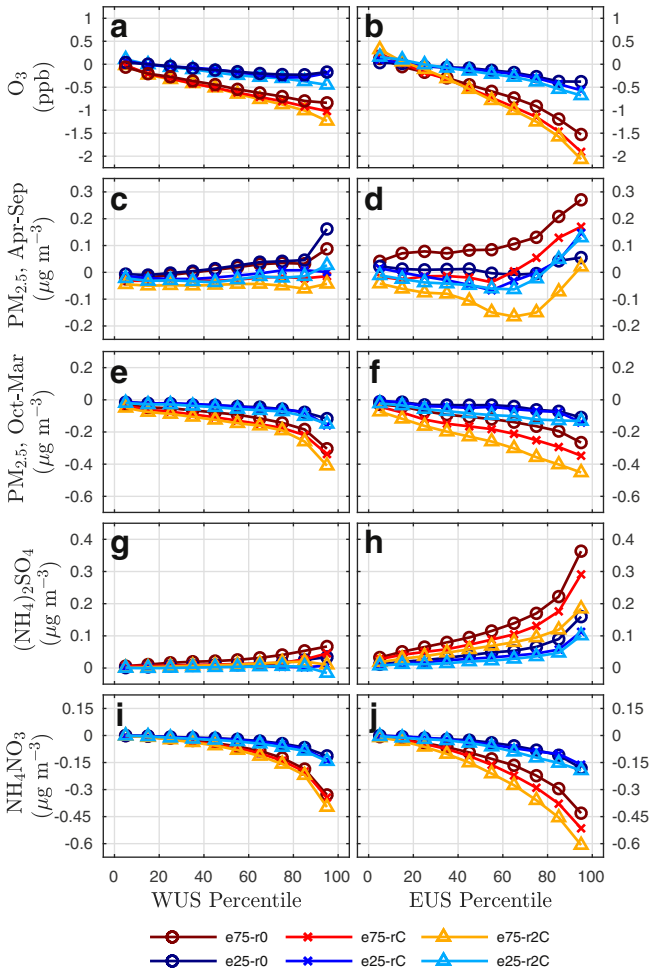

Fig. 3. Air quality changes binned at each 10th percentile and averaged over the WUS (left column, west of 100°W) and EUS (right column, east of 100°W) for each EV adoption scenario (colors) shown for (a, b) O_3, (c, d) $PM_{2.5}$ for April–September, (e, f) $PM_{2.5}$ for October–March, (g, h) $(NH_4)_2SO_4$, and (i, j) NH_4NO_3. (For interpretation of the references to color in this figure legend, the reader is referred to the Web version of this article.)

has the largest impact on high percentiles of O_3 (Fig. 3b), consistent with previous work over California (Razeghi et al., 2016).

Changes in $PM_{2.5}$ (Fig. 3c–f) are more nuanced than O_3 and depend on the season considered, resulting from competing effects of increases in $(NH_4)_2SO_4$ and reductions in NH_4NO_3. Due to this and the bimodal annual cycle of $PM_{2.5}$, we separate the $PM_{2.5}$ probability distribution into extended summer (April–September, Fig. 3c–d) and extended winter (October–March, Fig. 3e–f) to better describe $PM_{2.5}$ changes. The non-traditional 'season' definitions ensure each value is included in the calculations. Like O_3, the largest $PM_{2.5}$ changes occur at the high end of the distribution. In summer, $PM_{2.5}$ is largely controlled by changes in $(NH_4)_2SO_4$ (and OM) and thus mostly increases except for *e75-rC* and *e75-r2C* over the WUS and *e75-r2C* over the EUS. The largest increases generally occur for the combustion-only scenarios (i.e., *e75-r0*, *e25-r0*), highlighting the stronger influence of electricity generation type on resultant summer $PM_{2.5}$ as compared to O_3. This effect is more evident over the EUS. Winter $PM_{2.5}$ is dominated by NH_4NO_3 and as such decreases due to large reductions in NH_4NO_3, especially at high percentiles; however caution is warranted interpreting this result as the model is biased high during winter. In any case, the summer-winter disparity in $PM_{2.5}$ changes emphasizes an important point: summer $PM_{2.5}$ is controlled more strongly by the source of electricity generation used to power EVs, but winter $PM_{2.5}$ can decrease even when only combustion sources power EVs so long as the EV market penetration is high enough.

4. Conclusions and discussion

The scientific effort to quantify the environmental impact of EV adoption has largely paralleled the increasing global EV market share and has generally revealed that EVs offer a net environmental benefit (IEA, 2018; Requia et al., 2018). Using an emission remapping algorithm and a state-of-the-art chemistry-climate model, we have explored a range of scenarios to estimate the potential impact on U.S. air quality resulting from an aggressive transition from conventional, internal combustion, light-duty passenger vehicles to battery-powered electric vehicles. It is difficult to quantitatively compare results across studies due to wide ranging assumptions, model parameters, and disparate methodologies (e.g., spatial and temporal range, EV type, electricity generation types, emission remapping model, etc.); overall, however, our estimates for emission changes and resulting modeled air quality changes are similar to other comparable studies that have examined the electrification of transportation over the U.S. using a CTM (Tessum et al., 2014; EPRI, 2015; Nopmongcol et al., 2017).

Our method and results reveal the differing sensitivities of some measures of air quality to the reductions in the existing fleet's emissions and the type of power generation used to power a hypothetical EV fleet. We find that average summer O_3 abundances will decrease as EVs continue to make up a larger share of the U.S. vehicle fleet, regardless of the source of the electricity that charges them. A more aggressive transition to EVs results in greater O_3 reductions. The largest O_3 decreases are simulated at the extremes of the probability distribution and in the most polluted locations. Changes in $PM_{2.5}$ abundances are spatially, temporally, and scenario dependent. Summer $PM_{2.5}$ generally increases due to increased $(NH_4)_2SO_4$, but decreased winter $PM_{2.5}$ is found for almost all locations because of larger reductions in NH_4NO_3. Ultimately, the number of conventional vehicles replaced by EVs has a larger effect on O_3 than $PM_{2.5}$, while the source of the electricity for those EVs exhibit greater control on $PM_{2.5}$. Thus, if the displacement of the combustion engine with battery power outpaces the expansion of renewable energy sources for power generation, air pollution – particularly from fine particulate matter – may worsen until cleaner fuels are adopted.

Due to the novelty of the emission remapping methods, we have developed emissions for simulations at coarser resolutions (time and space) compared to most regional CTMs ($\sim$50 km vs. 4 km; monthly vs. hourly prescribed emissions) in an effort to limit complexity and reduce assumptions while still demonstrating utility of the methods. For example, a finer scale analysis would likely need to incorporate the impacts of both time-of-day driving and charging in order to match other urban-rural disparities illuminated by higher-resolutions. For example, we assume EVs are charged and thus the marginal electric demand is co-located with where the EVs are driven, which is likely a less valid assumption as resolution increases. Future work at higher resolutions can and should attempt to incorporate these processes.

A key limitation in accurately quantifying emission and air quality changes from EV adoption is the lack of open-source data and tools needed to determine where the marginal electric load will be allocated and, subsequently, the magnitude of the allocated power generation facility emissions. While so-called dispatch models exist, they are typically proprietary and/or only cover small geographic regions. Moreover, without publicly available and regularly updated data on the structure and details of the power grid, these types of models will likely remain proprietary and regionally focused. Our method circumvents this restriction, albeit with its own limitations. However, used in conjunction with open-source databases such as the Global Power Plant Database (Byers et al., 2018), it offers the potential for research beyond the U.S., where relatively little effort has been focused (Requia et al., 2018) despite more aggressive and near-term EV adoption targets.

Declarations of interest

None.

Acknowledgments

Research at Northwestern University was supported by the Ubben Program for Carbon and Climate Science (JLS) and the U.S. National Science Foundation grant CBET-1848683 (DEH).

Appendix A. Supplementary data

Supplementary data to this article can be found online at https://doi.org/10.1016/j.atmosenv.2019.04.003.

References

Alhajeri, N.S., McDonald-Buller, E.C., Allen, D.T., 2011. Comparisons of air quality impacts of fleet electrification and increased use of biofuels. Environ. Res. Lett. 6. https://doi.org/10.1088/1748-9326/6/2/024011.

Ansari, A.S., Pandis, S.N., 1998. Response of inorganic $PM_{2.5}$ to precursor concentrations. Environ. Sci. Technol. 32, 2706–2714. https://doi.org/10.1021/es971130j.

Brinkman, G.L., Denholm, P., Hannigan, M.P., Milford, J.B., 2010. Effects of plug-in hybrid electric vehicles on ozone concentrations in Colorado. Environ. Sci. Technol. 44, 6256–6262. https://doi.org/10.1021/es101076c.

Byers, L., Friedrich, J., Hennig, R., Kressig, A., Li, X., McCormick, C., Valeri, L.M., 2018. A Global Database of Power Plants. World Resources Institute, Washington, DC Available online at. www.wri.org/publication/global-database-power-plants.

Cai, H., Wang, M., 2014. Estimation of Emission Factors of Particulate Black Carbon and Organic Carbon from Stationary, Mobile, and Non-point Sources in the United States for Incorporation into GREET. Available at. https://greet.es.anl.gov/publication-black-carbon-greet, Accessed date: 5 July 2017.

Chen, J., Wang, W., Liu, H., Ren, L., 2012. Determination of road dust loadings and chemical characteristics using resuspension. Environ. Monit. Assess. 184, 1693–1709. https://doi.org/10.1007/s10661-011-2071-1.

Delucchi, M.A., 2000. Environmental externalities of motor-vehicle use in the US. J. Transp. Econ. Policy 34, 135–168.

Donner, L.J., Wyman, B.L., Hemler, R.S., Horowitz, L.W., Ming, Y., Zhao, M., Golaz, J.C., Ginoux, P., Lin, S.J., Schwarzkopf, M.D., Austin, J., Alaka, G., Cooke, W.F., Delworth, T.L., Freidenreich, S.M., Gordon, C.T., Griffies, S.M., Held, I.M., Hurlin, W.J., Klein, S.A., Knutson, T.R., Langenhorst, A.R., Lee, H.C., Lin, Y.L., Magi, B.I., Malyshev, S.L., Milly, P.C.D., Naik, V., Nath, M.J., Pincus, R., Ploshay, J.J., Ramaswamy, V., Seman, C.J., Shevliakova, E., Sirutis, J.J., Stern, W.F., Stouffer, R.J., Wilson, R.J., Winton, M., Wittenberg, A.T., Zeng, F.R., 2011. The dynamical core, physical parameterizations, and basic simulation characteristics of the atmospheric component AM3 of the GFDL global coupled model CM3. J. Clim. 24, 3484–3519. https://doi.org/10.1175/2011JCLI3955.1.

Duncan, B.N., Yoshida, Y., Olson, J.R., Sillman, S., Martin, R.V., Lamsal, L., Hu, Y.T., Pickering, K.E., Retscher, C., Allen, D.J., Crawford, J.H., 2010. Application of OMI observations to a space-based indicator of NOx and VOC controls on surface ozone formation. Atmos. Environ. 44, 2213–2223. https://doi.org/10.1016/j.atmosenv.2010.03.010d.

Environmental Assessment of On-Road Vehicle and Off-Road Equipment Electrification: Volume 3: Air Quality Impacts. EPRI, Palo Alto, CA, pp. 3002006880.

Ginoux, P., Chin, M., Tegen, I., Prospero, J.M., Holben, B., Dubovik, O., Lin, S.-J., 2001. Sources and distribution of dust aerosols simulated with the GOCART model. J. Geophys. Res. 106, 22255–22274.

Hill, J., Polasky, S., Nelson, E., Tilman, D., Huo, H., Ludwig, L., Neumann, J., Zheng, H.C., Bonta, D., 2009. Climate change and health costs of air emissions from biofuels and gasoline. Proc. Natl. Acad. Sci. U.S.A. 106, 2077–2082. https://doi.org/10.1073/pnas.0812835106.

Hoesly, R.M., Smith, S.J., Feng, L., Klimont, Z., Janssens-Maenhout, G., Pitkanen, T., Seibert, J.J., Vu, L., Andres, R.J., Bolt, R.M., Bond, T.C., Dawidowski, L., Kholod, N., Kurokawa, J.I., Li, M., Liu, L., Lu, Z., Moura, M.C.P., O'Rourke, P.R., Zhang, Q., 2017. Historical (1750–2014) anthropogenic emissions of reactive gases and aerosols from the Community Emission Data System (CEDS). Geosci. Model Dev. Discuss. 2017, 1–41. https://doi.org/10.5194/gmd-11-369-2018.

Huo, H., Zhang, Q., Liu, F., He, K.B., 2013. Climate and environmental effects of electric vehicles versus compressed natural gas vehicles in China: a life-cycle analysis at provincial level. Environ. Sci. Technol. 47, 1711–1718. https://doi.org/10.1021/es303352x.

Huo, H., Cai, H., Zhang, Q., Liu, F., He, K., 2015. Life-cycle assessment of greenhouse gas and air emissions of electric vehicles: a comparison between China and the U.S. Atmos. Environ. 108, 107–116. https://doi.org/10.1016/j.atmosenv.2015.02.073.

IEA, 2018. Global EV outlook: towards cross-modal electrification. International energy agency, clean energy ministerial, electric vehicles initiative. Available at. https://webstore.iea.org/global-ev-outlook-2018, Accessed date: 31 May 2018.

Intergovernmental Panel on Climate Change, 2014. Summary for policymakers. Climate change 2014: impacts, adaptation, and vulnerability. Part A: global and sectoral aspects. In: Field, C.B. (Ed.), Contribution of Working Group II to the Fifth Assessment

Report of the Intergovernmental Panel on Climate Change. Cambridge Univ Press, Cambridge, UK.
Jacobson, M.Z., 2009. Review of solutions to global warming, air pollution, and energy security. Energy Environ. Sci. 2, 148–173. https://doi.org/10.1039/b809990c.
Ji, S.G., Cherry, C.R., Bechle, M.J., Wu, Y., Marshall, J.D., 2012. Electric vehicles in China: emissions and health impacts. Environ. Sci. Technol. 46, 2018–2024. https://doi.org/10.1021/es202347q.
Ji, S.G., Cherry, C.R., Zhou, W.J., Sawhney, R., Wu, Y., Cai, S.Y., Wang, S.X., Marshall, J.D., 2015. Environmental justice aspects of exposure to PM2.5 emissions from electric vehicle use in China. Environ. Sci. Technol. 49, 13912–13920. https://doi.org/10.1021/acs.est.5b04927.
Jin, X., Fiore, A.M., Murray, L.T., Valin, L.C., Lamsal, L.N., Duncan, B., Boersma, K.F., Smedt, I.D., Abad, G.G., Chance, K., Tonnesen, G.S., 2017. Evaluating a space-based indicator of surface ozone-NO_x-VOC sensitivity over midlatitude source regions and applications to decadal trends. J. Geophys. Res. Atmos. 122 (19), 10439–10461. https://doi.org/10.1002/2017JD026720.
Li, N., Chen, J.P., Tsai, I.C., He, Q.Y., Chi, S.Y., Lin, Y.C., Fu, T.M., 2016. Potential impacts of electric vehicles on air quality in Taiwan. Sci. Total Environ. 566, 919–928. https://doi.org/10.1016/j.scitotenv.2016.05.105.
Li, J., Mao, J., Fiore, A.M., Cohen, R.C., Crounse, J.D., Teng, A.P., Wennberg, P.O., Lee, B.H., Lopez-Hilfiker, F.D., Thornton, J.A., Peischl, J., Pollack, I.B., Ryerson, T.B., Veres, P., Roberts, J.M., Neuman, J.A., Nowak, J.B., Wolfe, G.M., Hanisco, T.F., Fried, A., Singh, H.B., Dibb, J., Paulot, F., Horowitz, L.W., 2018. Decadal changes in summertime reactive oxidized nitrogen and surface ozone over the Southeast United States. Atmos. Chem. Phys. 18, 2341–2361. https://doi.org/10.5194/acp-18-2341-2018.
Lin, M., Fiore, A.M., Horowitz, L.W., Cooper, O.R., Naik, V., Holloway, J., Johnson, B.J., Middlebrook, A.M., Oltmans, S.J., Pollack, I.B., Ryerson, T.B., Warner, J.X., Wiedinmyer, C., Wilson, J., Wyman, B., 2012. Transport of Asian ozone pollution into surface air over the western United States in spring. J. Geophys. Res. Atmos. 117 (D00V07). https://doi.org/10.1029/2011JD016961.
Marais, E.A., Jacob, D.J., Jimenez, J.L., Campuzano-Jost, P., Day, D.A., Hu, W., Krechmer, J., Zhu, L., Kim, P.S., Miller, C.C., Fisher, J.A., Travis, K., Yu, K., Hanisco, T.F., Wolfe, G.M., Arkinson, H.L., Pye, H.O.T., Froyd, K.D., Liao, J., McNeill, V.F., 2016. Aqueous-phase mechanism for secondary organic aerosol formation from isoprene: application to the southeast United States and co-benefit of SO2 emission controls. Atmos. Chem. Phys. 16, 1603–1618. https://doi.org/10.5194/acp-16-1603-2016.
Michalek, J.J., Chester, M., Jaramillo, P., Samaras, C., Shiau, C.S.N., Lave, L.B., 2011. Valuation of plug-in vehicle life-cycle air emissions and oil displacement benefits. Proc. Natl. Acad. Sci. U.S.A. 108, 16554–16558. https://doi.org/10.1073/pnas.1104473108.
Naik, V., Horowitz, L.W., Fiore, A.M., Ginoux, P., Mao, J., Aghedo, A.M., Levy, H., 2013. Impact of preindustrial to present-day changes in short-lived pollutant emissions on atmospheric composition and climate forcing. J. Geophys. Res. Atmos. 118, 8086–8110. https://doi.org/10.1002/jgrd.50608.
Nichols, B.G., Kockelman, K.M., Reiter, M., 2015. Air quality impacts of electric vehicle adoption in Texas. Trans. Res. D Transp. Environ. 34, 208–218. https://doi.org/10.1016/j.trd.2014.10.016.
Nopmongcol, U., Grant, J., Knipping, E., Alexander, M., Schurhoff, R., Young, D., Jung, J., Shah, T., Yarwood, G., 2017. Air quality impacts of electrifying vehicles and equipment across the United States. Environ. Sci. Technol. 51, 2830–2837. https://doi.org/10.1021/acs.est.6b04868.
Paulot, F., Ginoux, P., Cooke, W.F., Donner, L.J., Fan, S., Lin, M.-Y., Mao, J., Naik, V., Horowitz, L.W., 2016. Sensitivity of nitrate aerosols to ammonia emissions and to nitrate chemistry: implications for present and future nitrate optical depth. Atmos. Chem. Phys. 16, 1459–1477. https://doi.org/10.5194/acp-16-1459-2016.
Paulot, F., Fan, S., Horowitz, L.W., 2017. Contrasting seasonal responses of sulfate aerosols to declining SO_2 emissions in the Eastern U.S.: implications for the efficacy of SO_2 emission controls. Geophys. Res. Lett. 44, 455–464. https://doi.org/10.1002/2016GL070695.
Razeghi, G., Carreras-Sospedra, M., Brown, T., Brouwer, J., Dabdub, D., Samuelsen, S., 2016. Episodic air quality impacts of plug-in electric vehicles. Atmos. Environ. 137, 90–100. https://doi.org/10.1016/j.atmosenv.2016.04.031.
Requia, W.J., Mohamed, M., Higgins, C.D., Arain, A., Ferguson, M., 2018. How clean are electric vehicles? Evidence-based review of the effects of electric mobility on air pollutants, greenhouse gas emissions and human health. Atmos. Environ. 185, 64–77. https://doi.org/10.1016/j.atmosenv.2018.04.040.
Schnell, J.L., Prather, M.J., 2017. Co-occurrence of extremes in surface ozone, particulate matter, and temperature over eastern North America. Proc. Natl. Acad. Sci. U.S.A. 114, 2854–2859. https://doi.org/10.1073/pnas.1614453114. 2017.
Schnell, J.L., Naik, V., Horowitz, L.W., Paulot, F., Mao, J., Ginoux, P., Zhao, M., Ram, K., 2018. Exploring the relationship between surface $PM_{2.5}$ and meteorology in Northern India. Atmos. Chem. Phys. 18, 10157–10175. https://doi.org/10.5194/acp-18-10157-2018.
Seinfeld, J.H., 1986. Atmospheric Chemistry and Physics of Air Pollution. Wiley, New York.
Simons, A., 2016. Road transport: new life cycle inventories for fossil-fuelled passenger cars and non-exhaust emissions in ecoinvent v3. Int. J. Life Cycle Assess. 21, 1299–1313. https://doi.org/10.1007/s11367-013-0642-9.
Stelson, A.W., Seinfeld, J.H., 1982. Relative humidity and temperature dependence of the ammonium nitrate dissociation constant. Atmos. Environ. 16 (5), 983–992. https://doi.org/10.1016/0004-6981(82)90184-6.
Tessum, C.W., Hill, J.D., Marshall, J.D., 2014. Life cycle air quality impacts of conventional and alternative light-duty transportation in the United States. Proc. Natl. Acad. Sci. U.S.A. 111, 18490–18495. https://doi.org/10.1073/pnas.1406853111.
Thompson, T., Webber, M., Allen, D.T., 2009. Air quality impacts of using overnight electricity generation to charge plug-in hybrid electric vehicles for daytime use. Environ. Res. Lett. 4. https://doi.org/10.1088/1748-9326/4/1/014002.
Thompson, T.M., King, C.W., Allen, D.T., Webber, M.E., 2011. Air quality impacts of plug-in hybrid electric vehicles in Texas: evaluating three battery charging scenarios. Environ. Res. Lett. 6. https://doi.org/10.1088/1748-9326/6/2/024004.
Timmers, V.R.J.H., Achten, P.A.J., 2016. Non-exhaust PM emissions from electric vehicles. Atmos. Environ. 134, 10–17. https://doi.org/10.1016/j.atmosenv.2016.03.017.
US Department of Transportation, 2017. Table 1-35: U.S. Vehicle miles. Available at. https://www.bts.gov/archive/publications/national_transportation_statistics/table_01_35, Accessed date: 18 March 2018.
US Environmental Protection Agency, 2008. Average annual emissions and fuel consumption for gasoline-fueled passenger cars and light trucks emission facts. Available at: https://nepis.epa.gov/Exe/ZyPURL.cgi?Dockey=P100EVXP.TXT, Accessed date: 18 March 2018.
US Environmental Protection Agency, 2014. 2014 national emissions inventory (NEI). Available at: https://www.epa.gov/air-emissions-inventories/2014-national-emissions-inventory-nei-data, Accessed date: 15 March 2018.
US Environmental Protection Agency, 2017. 2014 eGRID Database. Available at: https://www.epa.gov/energy/emissions-generation-resource-integrated-database-egrid, Accessed date: 20 July 2017.
van Marle, M.J.E., Kloster, S., Magi, B.I., Marlon, J.R., Daniau, A.L., Field, R.D., Arneth, A., Forrest, M., Hantson, S., Kehrwald, N.M., Knorr, W., Lasslop, G., Li, F., Mangeon, S., Yue, C., Kaiser, J.W., van der Werf, G.R., 2017. Historic global biomass burning emissions based on merging satellite observations with proxies and fire models (1750-2015). Geosci. Model Dev. Discuss. (GMDD) 1–56. https://doi.org/10.5194/gmd-2017-32. 2017.
Weis, A., Michalek, J.J., Jaramillo, P., Lueken, R., 2015. Emissions and cost implications of controlled electric vehicle charging in the US PJM interconnection. Environ. Sci. Technol. 49, 5813–5819. https://doi.org/10.1021/es505822f.
Wu, Y., Zhang, L., 2017. Can the development of electric vehicles reduce the emission of air pollutants and greenhouse gases in developing countries? Trans. Res. D Transp. Environ. 51, 129–145. https://doi.org/10.1016/j.trd.2016.12.007.
Young, P.J., Naik, V., Fiore, A.M., Gaudel, A., Guo, J., Lin, M.Y., Neu, J.L., Parrish, D.D., Rieder, H.E., Schnell, J.L., Tilmes, S., Wild, O., Zhang, L., Ziemke, J., Brandt, J., Delcloo, A., Doherty, R.M., Geels, C., Hegglin, M.I., Hu, L., Im, U., Kumar, R., Luhar, A., Murray, L., Plummer, D., Rodriguez, J., Saiz-Lopez, A., Schultz, M.G., Woodhouse, M.T., Zeng, G., 2018. Tropospheric Ozone Assessment Report: assessment of global-scale model performance for global and regional ozone distributions, variability, and trends. Elementa-Sci. Anthro. 6. https://doi.org/10.1525/elementa.265.
Zhao, M., Golaz, J.C., Held, I.M., Guo, H., Balaji, V., Benson, R., Chen, J.H., Chen, X., Donner, L.J., Dunne, J.P., Dunne, K., Durachta, J., Fan, S.M., Freidenreich, S.M., Garner, S.T., Ginoux, P., Harris, L.M., Horowitz, L.W., Krasting, J.P., Langenhorst, A.R., Liang, Z., Lin, P., Lin, S.J., Malyshev, S.L., Mason, E., Milly, P.C.D., Ming, Y., Naik, V., Paulot, F., Paynter, D., Phillipps, P., Radhakrishnan, A., Ramaswamy, V., Robinson, T., Schwarzkopf, D., Seman, C.J., Shevliakova, E., Shen, Z., Shin, H., Silvers, L.G., Wilson, J.R., Winton, M., Wittenberg, A.T., Wyman, B., Xiang, B., 2018a. The GFDL global atmosphere and land model am4.0/lm4.0:1. Simulation characteristics with prescribed SSTs. J. Adv. Model. Earth Syst. 10, 691–734. https://doi.org/10.1002/2017ms001208.
Zhao, M., Golaz, J.C., Held, I.M., Guo, H., Balaji, V., Benson, R., Chen, J.H., Chen, X., Donner, L.J., Dunne, J.P., Dunne, K., Durachta, J., Fan, S.M., Freidenreich, S.M., Garner, S.T., Ginoux, P., Harris, L.M., Horowitz, L.W., Krasting, J.P., Langenhorst, A.R., Liang, Z., Lin, P., Lin, S.J., Malyshev, S.L., Mason, E., Milly, P.C.D., Ming, Y., Naik, V., Paulot, F., Paynter, D., Phillipps, P., Radhakrishnan, A., Ramaswamy, V., Robinson, T., Schwarzkopf, D., Seman, C.J., Shevliakova, E., Shen, Z., Shin, H., Silvers, L.G., Wilson, J.R., Winton, M., Wittenberg, A.T., Wyman, B., Xiang, B., 2018b. The GFDL global atmosphere and land model am4.0/lm4.0:2. Model description, sensitivity studies, and tuning strategies. J. Adv. Model. Earth Syst. 10, 735–769. https://doi.org/10.1002/2017ms001209.
Zivin, J.S.G., Kotchen, M.J., Mansur, E.T., 2014. Spatial and temporal heterogeneity of marginal emissions: implications for electric cars and other electricity-shifting policies. J. Econ. Behav. Organ. 107, 248–268. https://doi.org/10.1016/j.jebo.2014.03.010.